Frequency-constrained energy and reserve scheduling in wind incorporated low-inertia power systems considering vanadium flow redox batteries

Received: 29 May 2022 | Revised: 19 July 2022 | Accepted: 30 July 2022

IET Generation, Transmission & Distribution

DOI: 10.1049/gtd2.12592

The Institution of Engineering and Technology WILEY

ORIGINAL RESEARCH

Frequency-constrained energy and reserve scheduling in wind incorporated low-inertia power systems considering vanadium flow redox batteries

Maryam Mohiti[1] | **Mohammadreza Mazidi**[1,2] | **Mostafa Kermani**[1] | **Davoud Abootorabi Zarchi**[2]

[1]Department of Electrical Engineering, Chalmers University of Technology, Göteborg, Sweden

[2]Department of Electrical Engineering, Yazd University, Yazd, Iran

Correspondence
Mohammadreza Mazidi, Chalmers University of Technology, 412 96 Göteborg, Sweden
Email: mazadi@chalmers.se

Abstract

This paper proposes a novel energy and reserve scheduling model for power systems with high penetration of wind turbines (WTs). The objective of the proposed model is to minimize the total operation cost of the system while static and dynamic security is guaranteed by preserving the frequency nadir, RoCoF, and quasi-steady-state frequency in the predefined range. Likewise, a supervisory, control, and data acquisition (SCADA) system is developed which allows Vanadium Redox Flow Batteries (VRFBs) to continuously communicate and participate in the primary frequency response. To cope with the uncertainties, adaptive information gap decision theory is used that ensures a target operating cost for the risk-averse operator of the power system. The proposed scheduling model is applied on a modified IEEE 39 bus test system to verify the impacts of the fast reserve provided by the VRFBs in the dynamic frequency security enhancement of the power system with high penetration of WTs.

1 | INTRODUCTION

The integration of renewable energy sources such as wind turbines (WTs) in the power system has increased significantly. Unlike the synchronous generators (SGs), WTs are connected to the power system through power electronic converters that lead to a noticeable reduction in the system inertia [1]. These beside uncertainties associated with generation power of WTs lead to frequency excursions which impose severe challenges to operators of power systems in maintaining frequency security [2]. Thus, it is needed to develop operation models in which frequency security along with uncertainties are considered in power systems with high penetration level of WTs.

Frequency security has been defined by National Grid standards in metrics of rate of change of frequency (RoCoF), frequency nadir, and quasi-steady-state frequency [3]. Accordingly, there have been some previous efforts to establish frequency constrained unit commitment (FCUC) to include frequency security in power system scheduling problem. A stochastic-based FCUC model for virtual inertia response provision from WTs and primary response from SGs governor to preserve RoCoF and frequency nadir in the secure ranges has been proposed in [4]. A security margin in terms of maximum permissible power imbalance to quantify the system frequency response in the proposed FCUC model is introduced in [5]. A piecewise linear technique in [5] has been applied to linearize the presented frequency response model to facilitate its integration in the FCUC. Also, a linearized metrics of dynamic and steady-state frequency security in the FCUC model is unified in [6]. In [7], frequency excursions resulting from different system contingencies have been studied in the FCUC problem of an isolated power system with the WTs contribution for frequency stability enhancement.

The aforementioned works have made significant contribution in incorporating frequency security in the FCUC problem; however, with fast response of battery energy storage systems (BESSs), power mismatch and preserving frequency security problems can be addressed by them. In some other works,

the BESSs are considered in the energy and reserve scheduling problem [10–12]. Also, in [8] the BESS is involved in the UC problem to improve the frequency security of the system as well as providing energy arbitrage in normal operation of the system, while it is assumed after a contingency the BESS inject all its energy to provide frequency support. In [9], a probabilistic UC model is developed by incorporating BESS and wind energy in the problem. A deterministic UC is used to co-optimize energy storage and UC scheduling decisions for cost saving and energy arbitrage [10]. In these works, although the BESS is considered in the UC problem, however, to the best of authors' knowledge there has been no previous research which has incorporated the BESSs in both energy and reserve scheduling. To cope with these drawbacks in this paper the BESS participates in the frequency regulation of the system by providing energy and primary reserves. In the proposed model the BESS is optimally coordinated with the WTs to provide both energy and reserve to compensate frequency excursions.

The short interval of primary frequency control necessitates the BESS technology to be selected to have a very fast response time and charge/discharge rate. Vanadium Redox Flow Batteries (VRFBs) are one of the recent and most promising technologies for stationary BESSs in the power system [11]. VRFBs exhibit several key advantages over other BESS technologies; their scalability and independent power and energy rating makes them an appealing choice for large-scale utilization [12]. VRFB's fast response time, high charge/discharge rate, and low self-discharge enable them to participate in frequency regulation by providing fast reserve in comparison with other types of BESSs [13]. In [14], to enhance the efficiency of the VRFBs under real-world grid operating conditions, a two-stage optimal control strategy is proposed. The strategy demonstrates high efficiency and high accuracy in tracking dynamic power profiles to smooth renewable generation. In [15], a control strategy is conducted for a VRFB as an energy storage device to smooth the wind farm out-put fluctuation. The results have shown that the output power of wind farm is well regulated at specified levels. In [16], the fast discharge of VRFBs in various operating conditions was carried out with the aim of exploring the capability of these batteries to provide fast grid services.

As mentioned earlier, the associated uncertainties of WTs and the resulting power mismatch can lead to power system frequency excursions. To tackle this issue, the uncertainties of the WTs should be properly modelled in the UC problem. Several approaches have been used in the literature to deal with uncertainties which each have their pros and cons. Stochastic optimization has been used in the UC problem in [17]. Stochastic optimization approaches (SOA) utilize a scenario-based representation of uncertainties along with their associated probabilities [18]. As SOA need probability functions of uncertain variables, its optimality depends on the accuracy of the probability distribution functions (PDFs) and the number of scenarios. Therefore, insufficient historic data can lead to inaccurate PDFs and non-optimal solutions [19]. To cope with these issues, robust optimization approaches (ROAs) are introduced. In ROAs the lower and upper bands for the uncertain variable are defined as uncertainty sets and the uncertain variable can vary in this interval [20]. However, ROAs optimize the objective function for the worst case scenario and their solutions are exposed to over-conservativeness [21]. Information Gap Decision Theory (IGDT) approach is a non-probabilistic robust optimization method in which, unlike ROA and SOAs the PDF of uncertain variables or their margins are not available. In IGDT, the maximum discrepancy of uncertainty is obtained according to the risk-averse and risk-seeker strategies of the decision makers. So, the robustness of the uncertain variables is calculated [22]. In [23], the IGDT approach has been used to model the UC problem in power systems with high penetration of WTs. A security-constrained UC model considering lithium-ion energy storage in which the uncertainty of load demand is handled by the IGDT approach is proposed in [24]. In [25], an IGDT-stochastic approach has been utilized to model a UC problem with electric vehicle as mobile energy storage, demand response, and WTs without the frequency security of power system consideration. Likewise, in the IGDT approach the robustness band of the uncertain variables, e.g., power generation from WTs, is considered constant for the whole operating horizon. However, during the scheduling horizons the share of WTs in total system generation is relatively high in some hours which increases the uncertainty and the system is more vulnerable to the frequency excursions.

In this paper, a novel energy and reserve scheduling model for power systems with high penetration of WTs is developed in which the VRFBs are incorporated in both the energy and reserve scheduling. In the developed model, the VRFBs are coordinated with SGs to provide energy and reserve to minimize the total cost of the system while dynamic and static frequency security is assured. Frequency nadir, RoCoF, and quasi-steady-state frequency are used as metrics of static and dynamic frequency security of the power system. To cope with uncertainties in power generation from WTs, an adaptive IGDT (AIGDT) approach is used so that the robustness band is adaptive to the share of WTs in total system generation during the scheduling horizon. Consequently, a target operation cost is guaranteed for the risk-averse operator. The main contribution of this paper can be summarized as follows:

- Proposing a novel energy and reserve scheduling model for power systems with high penetration of WTs in which the VRFBs are incorporated in both the energy and reserve scheduling.
- Optimal participation of VRFBs in primary frequency control by providing reserve in the primary frequency interval. Accordingly, the static and dynamic security of the system is assured by preserving the frequency nadir, RoCoF, and quasi-steady-state frequency in the predefined range.
- Considering WTs uncertainties by an adaptive IGDT (AIGDT) approach in which the robustness band is dynamically changed in every scheduling horizon.

The rest of this paper is organized as follows. The deterministic model for energy and reserve scheduling is presented in Section 2. The proposed model to consider uncertainty of WTs' power using AIGDT method is recast in Section 3. A case study

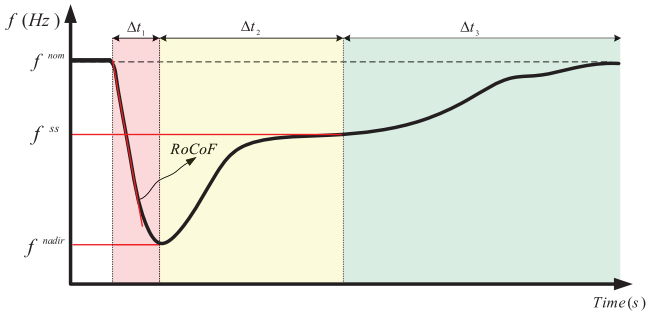

FIGURE 1 Frequency transition following a power shortage in the power systems. Δt_1 : inertia response, Δt_2 : primary frequency control, Δt_3 : secondary frequency control

with the proposed model is simulated and simulation results are discussed in Section 4. Finally, Section 5 concludes the paper.

2 | DETERMINISTIC MODEL FOR ENERGY AND RESERVE SCHEDULING

In this section the deterministic energy and reserve scheduling model is described. The developed model is modified based on the AIGDT approach to consider the uncertainties of WTs generation.

2.1 | Dynamic behaviour of power system

Following a major disturbance in the power systems, the frequency undergoes a transition which, as shown in Figure 1, has three stages. Right after a disturbance, the frequency begins to change which can be denoted by the swing equation of single-machine equivalent system [26]:

$$\frac{2H_{sys}}{f_0}\frac{d\Delta f(t)}{dt} = \frac{\left(\Delta Pm - \Delta P_g\right)}{S_{B,sys}} \tag{1}$$

where H_{sys} is the total system inertia and equals the sum of inertias from all committed SGs:

$$H_{sys} = \frac{\sum_i H(i)\, PG^{\max}(i)\, u(i)}{S_{B,sys}} \tag{2}$$

Since at the very beginning of the disturbance the mechanical power of prime movers remains constant ($\Delta Pm = 0$), only the inertia of SGs limits the dropping of frequency in the first stage (i.e., Δt_1) which takes a few seconds. Therefore, according to (1), the initial rate of change of frequency can be calculated as

$$RoCoF = \frac{d\Delta f(t)}{dt} = \frac{-\Delta P_d . f_0}{2H_{sys}S_{B,sys}} \tag{3}$$

After the inertia response, the governors of SGs automatically response to deliver primary frequency reserves (PFRs). Likewise, in this paper the charge/discharge power of VRFBs is adjusted to reduce the disturbance. Accordingly, as shown in Figure 1, the frequency variation is stopped and then stabilized at a new steady-state level. The duration of this stage is indicated by Δt_2 and referred to the primary frequency control.

The governor response during a disturbance can be modelled as following [27]:

$$\Delta Pm(t) = \pm\begin{cases} \frac{R_g}{T_d}t & t < T_d \\ R_g & t \geq T_d \end{cases} \tag{4}$$

According to (4), the generation of SGs is increased in the case of power shortage ($\Delta P_d > 0$) and reduced in the case of power abundance ($\Delta P_d < 0$). The frequency trajectory during a power shortage disturbance can be retrieved based on (1) as following:

$$f(t) = \frac{f_0 . R_p}{4H_{sys}S_{B,sys}}t^2 - \frac{\Delta P_d . f_0}{2H_{sys}S_{B,sys}}t + f_0 - \Delta f_{db} \tag{5}$$

The parameter R_p is the maximum ramp rate that the governor delivers the PFR. By deploying derivation, the frequency nadir (f^{nadir}) and nadir time (t^{nadir}) can be calculated as following:

$$f^{nadir} = f_0 - \Delta f_{db} - \frac{f_0 . \Delta P_d^2}{4H_{sys}S_{B,sys}R_p} \tag{6}$$

$$t^{nadir} = \frac{\Delta P_d}{R_p} + \frac{-\Delta f_{db}}{RoCoF} \tag{7}$$

Similarly, the frequency trajectory during a power abundance disturbance can be retrieved based on (1) as following:

$$f(t) = -\frac{f_0 . R_p}{4H_{sys}S_{B,sys}}t^2 - \frac{\Delta P_d . f_0}{2H_{sys}S_{B,sys}}t + f_0 + \Delta f_{db} \tag{8}$$

By deploying derivation, the frequency zenith and zenith time can be calculated as following:

$$f^{zenith} = f_0 + \Delta f_{db} + \frac{f_0 . \Delta P_d^2}{4H_{sys}S_{B,sys}R_p} \tag{9}$$

$$t^{zenith} = \frac{\Delta P_d}{R_p} + \frac{\Delta f_{db}}{RoCoF} \tag{10}$$

As shown in Figure 1, the deviated frequency is settled to a quasi-steady state in the second stage which can be calculated as following:

$$\Delta f^{ss} = \left(\Delta P_d - PFR^{tot}\right)/D \tag{11}$$

It should be noted that contribution of loads in the calculation of steady-state frequency has been considered. As indicated in (11), the frequency cannot be compensated to the

nominal value (i.e., 50 Hz) at the primary control stage; hence, the controllers change the set-points of SGs and their commitment status in the second stage to recover the frequency to the nominal value. The duration of this stage is indicated by Δt_3 and referred to the secondary frequency control. This stage is not considered in the proposed model of this paper.

2.2 | Objective function

The independent system operator (ISO) determines the optimal energy and reserve scheduling for 24-h time horizon to minimize total operation cost of system:

$$\begin{aligned} &\textit{Minimize Cost} \\ &= \sum_{t=1}^{NT}\sum_{i=1}^{NG}\Big(C^{SD}(i,t)v(i,t) + C^{SU}(i,t)w(i,t) \\ &+ C^{F}(i,t)u(i,t) + C^{V}(i)PG(i,t) + C^{up}(i)RG^{up}(i,t) \\ &+ C^{dn}(i)RG^{dn}(i,t)\Big) + \sum_{t=1}^{NT}\sum_{b=1}^{NV} C^{B}(b)\Big(P^{c}_{VRB}(b,t) \\ &+ P^{d}_{VRB}(b,t)\Big) + \sum_{t=1}^{NT}\sum_{n=1}^{NB} C^{ENS}(t)\,ENS(n,t) \\ &+ \sum_{t=1}^{NT}\sum_{n=1}^{NB} C^{EWS}(t)\,EWS(n,t) \end{aligned} \tag{12}$$

The first term of (12) is the operation cost of SGs which includes startup cost, shut-down cost, fuel cost, and reserve costs, respectively. Likewise, the second term of (12) is the operation cost of VRFBs. The two last terms are penalty costs due to load shedding and wind power curtailment, respectively.

2.3 | Constraints

The ISO should schedule the optimal energy and reserve in the power system subject to technical and economic constraints which are presented in the following.

2.3.1 | Power balance constraints

The power balance between generation and load at each period of scheduling should be obeyed. Accordingly, the following constraint is defined:

$$\begin{aligned} &\sum_{i=1}^{NG} PG(i,t) + \sum_{j=1}^{NW} PW(j,t) + \sum_{b=1}^{NV}\Big(P^{d}_{VRB}(b,t) - P^{c}_{VRB}(b,t)\Big) \\ &+ \sum_{n=1}^{NB} ENS(n,t) - \sum_{n=1}^{NB} EWS(n,t) = \sum_{n=1}^{NB} Load(n,t) \end{aligned} \tag{13}$$

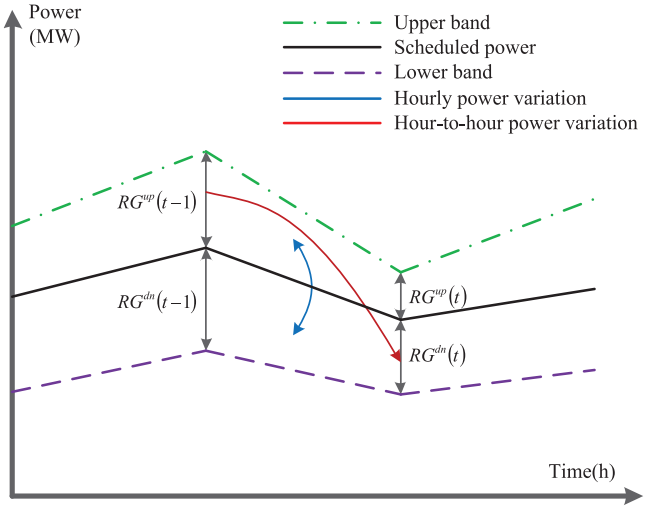

FIGURE 2 Ramping capability of SGs

2.3.2 | Transmission line capacity constraint

The power which flows through each transmission line of power system should be limited to its capacity. Accordingly, the following constraints are demonstrated:

$$\begin{aligned} -F^{max}(l) \le \sum_{n=1}^{NB} K(l,n)\Bigg(&\sum_{i\in\Omega^{G}_{n}} PG(i,t) + \sum_{j\in\Omega^{W}_{n}} PW(j,t) \\ &+ \sum_{b\in\Omega^{B}_{n}}\Big(P^{d}_{VRB}(b,t) - P^{c}_{VRB}(b,t)\Big) - Load(n,t)\Bigg) \le F^{max}(l) \end{aligned} \tag{14}$$

2.3.3 | Operational constraints of SGs

The committed SGs should accomplish several technical constraints which are formulated in this subsection. The maximum and minimum capacity limits are as following:

$$PG(i,t) + RG^{up}(i,t) \le PG^{max}(i)\,u(i,t) \tag{15}$$

$$PG(i,t) - RG^{dn}(i,t) \ge PG^{min}(i)\,u(i,t) \tag{16}$$

As shown in Figure 2, the upward and downward ramping capabilities of SGs should be adhered during any hour and hour-to-hour of scheduling horizon which are presented as following:

$$RG^{up}(i,t) + RG^{dn}(i,t) \le RG^{up\_max}(i)\,u(i,t) \tag{17}$$

$$RG^{up}(i,t) + RG^{dn}(i,t) \le RG^{dn\_max}(i)\,u(i,t) \tag{18}$$

$$PG(i,t) + RG^{up}(i,t) - PG(i,t-1) + RG^{dn}(i,t-1) \leq RU(i)\,u(i,t-1) + SU(i)(u(i,t) - u(i,t-1)) + \alpha(i)(1 - u(i,t)) \quad (19)$$

$$\alpha(i) = max\left(0, SU(i) - RU(i) - PG^{min}(i)\right) \quad (20)$$

$$PG(i,t-1) + RG^{up}(i,t-1) - PG(i,t) + RG^{dn}(i,t) \leq RD(i)\,u(i,t-1) + SD(i)(u(i,t-1) - u(i,t)) + \beta(i)(1 - u(i,t-1)) \quad (21)$$

$$\beta(i) = max\left(0, SD(i) - RD(i) - PG^{min}(i)\right) \quad (22)$$

According to (17–22), the variation in power of SGs from upper/lower band to lower/upper band can be guaranteed during any hour and hour-to-hour of scheduling horizon as shown in Figure 2.

A specified number of hours are required before SGs can be started up or shut down. These constraints are considered as follows:

$$\sum_{h=t-T^{up}(i)+1}^{t} w(i,h) \leq u(i,t);\ \forall t \in \left[T^{ON}(i), N_T\right] \quad (23)$$

$$\sum_{h=t-T^{dn}(i)+1}^{t} v(i,h) \leq 1 - u(i,t);\ \forall t \in \left[T^{\mathrm{OFF}}(i), N_T\right] \quad (24)$$

$$u(i,t) = u(i,0);\ \forall t \in \left[0, T^{ON}(i) + T^{\mathrm{Off}}(i)\right] \quad (25)$$

$$w(i,t) - v(i,t) = u(i,t) - u(i,t-1) \quad (26)$$

$$w(i,t) + v(i,t) \leq 1 \quad (27)$$

$$PG(i,t-1) + RG^{up}(i,t-1) - PG(i,t) + RG^{dn}(i,t) \leq RD(i)\,u(i,t-1) + SD(i)(u(i,t-1) - u(i,t)) + \beta(i)(1 - u(i,t-1)) \quad (28)$$

$$\beta(i) = max\left(0, SD(i) - RD(i) - PG^{\min}(i)\right) \quad (29)$$

2.3.4 | Operational constraints of VRFBs

VRFB is a flow battery which converts chemical energy to electricity, based on redox reactions of different ions of Vanadium in its electrolytes. As shown in Figure 3, reversible reactions of V^{2+}/V^{3+} and VO^{2+}/VO_2^+ occur in the cell stack. The electrolytes are stored in separate tanks and are circulated by pumps.

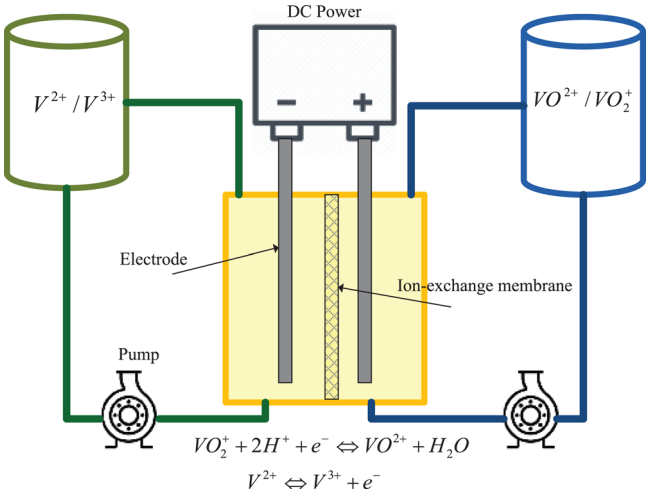

FIGURE 3 Schematic diagram of vanadium redox flow battery (VRFB)

The state of charge of VRFB can be modelled as (30) in the charge and discharge states:

$$SOC(b,t) = \begin{cases} SOC(b,t-1) - \int_{t-1}^{t} \dfrac{P_{VRB}^{d}(b,t)}{\eta_d(b,t)\,E^{rated}(b)}dt, & discharge \\ SOC(b,t-1) + \int_{t-1}^{t} \dfrac{P_{VRB}^{c}(b,t)\,\eta_c(b,t)}{E^{rated}(b)}dt, & charge \end{cases} \quad (30)$$

The losses of VRFB during charge/discharge are due to voltage stack losses and parasitic losses [28]. The cell stack of VRFBs is composed of a number of cells in series; however, the cell stack voltage is lower at higher discharge currents which is due to ohmic losses of internal resistances and activation and concentration losses of the electrolyte [29]. The parasitic losses account for the power which the VRFB should supply to its own pumps in addition to loads during discharge or the extra power should be provided by the grid for the pumps during charge mode. Therefore, the dynamic discharge and charge efficiency can be obtained as follows for each scheduling horizon according to [30]:

$$\eta_d(b,t) = \frac{P_{VRB}^{d,p.u}(b,t)}{\left(a_1^d(b)\,P_{VRB}^{d,p.u}(b,t) + b_1^d(b)\,SOC(b,t)\,(SOC(b,t)-1) + c_1(b)\right)} \quad (31)$$

$$\eta_c(b,t) = \frac{a_2(b)\,SOC(b,t) + b_2(b))P_{VRB}^{c}(b,t) + c_2(b)\,SOC(b,t) + d_2(b)}{P_{VRB}^{c,p.u}(b,t)} \quad (32)$$

The fitting parameters of charge and discharge related to the VRFB are retrieved from [30] and presented in Table 1:

As mentioned, the VRFB should supply the pump powers during charge and discharge. Hence, the maximum injected or absorbed power by the VRFB is restricted to P_{ab} [30].

$$P_{ab}^{d}(b,t) = a_3(b)\,SOC^2(b,t) + b_3(b)\,SOC(b,h) + c_3(b) \quad (33)$$

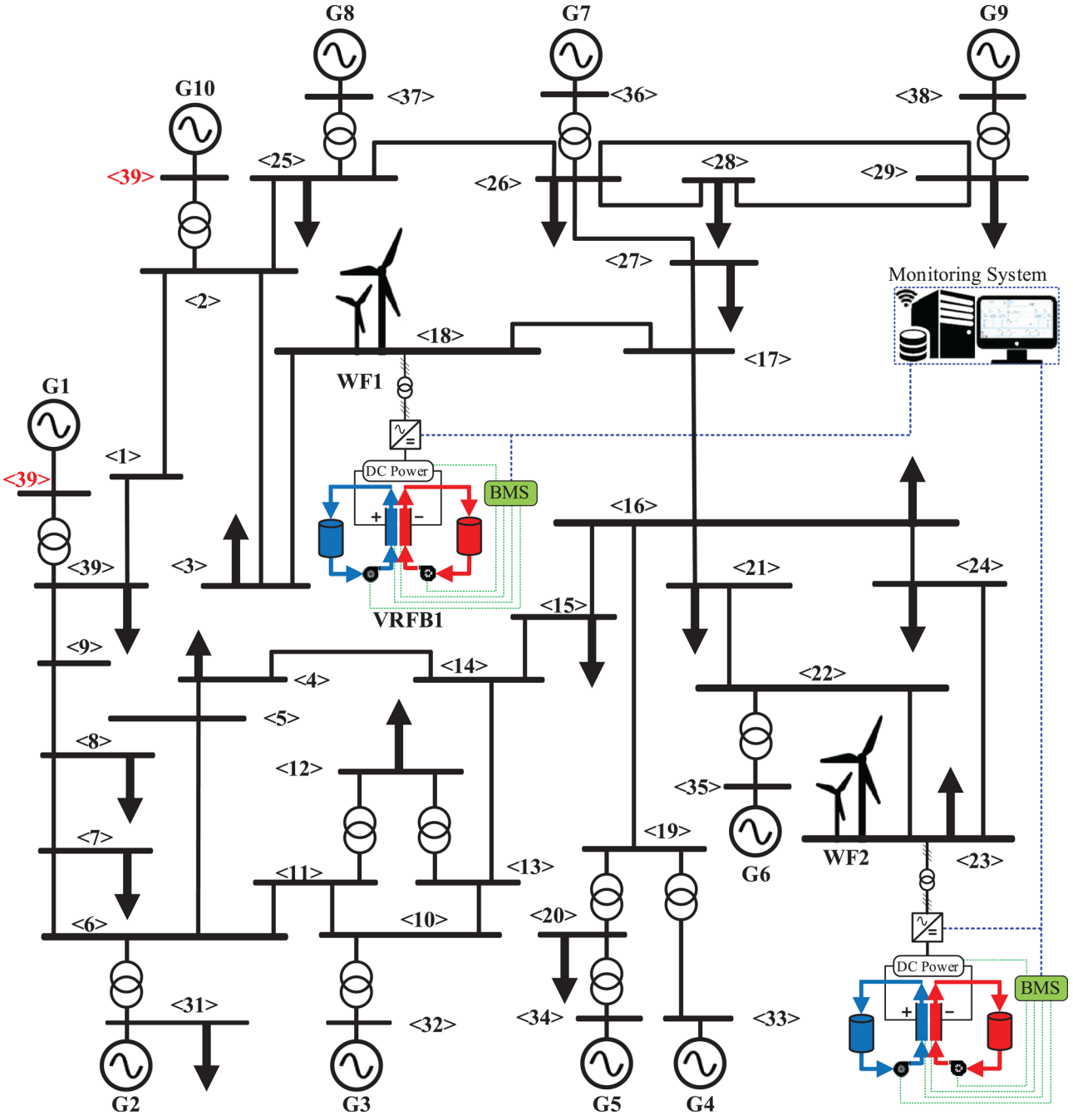

FIGURE 4 Single line diagram of the modified IEEE 39-bus test system

TABLE 1 Fitting parameters of charge/discharge efficiencies and absorb power

Parameter	a_i	b_i	c_i	d_i
$i = 1$	1.0334	0.3454	0.1192	–
$i = 2$	−0.128	1.05	0.038	0.118
$i = 3$	0.1686	0.8553	−0.0238	–
$i = 4$	0.5715	0.4605	−1.0321	–

$$P_{ab}^{d}(b,t) = a_3(v)\,SOC^2(b,t) + b_3(b)\,SOC(b,h) + c_3(b) \quad (34)$$

$$P_{VRB}^{d,p,u}(b,t) \le \left|P_{ab}^{d}(b,t)\right| u^{d}(b,t) \quad (35)$$

$$P_{VRB}^{c,p,u}(b,t) \le \left|P_{ab}^{c}(b,t)\right| u^{c}(b,t) \quad (36)$$

where the following constraint ensures the VRFB is not charged and discharge simultaneously.

$$u^{c}(b,t) + u^{d}(b,t) \le 1 \quad (37)$$

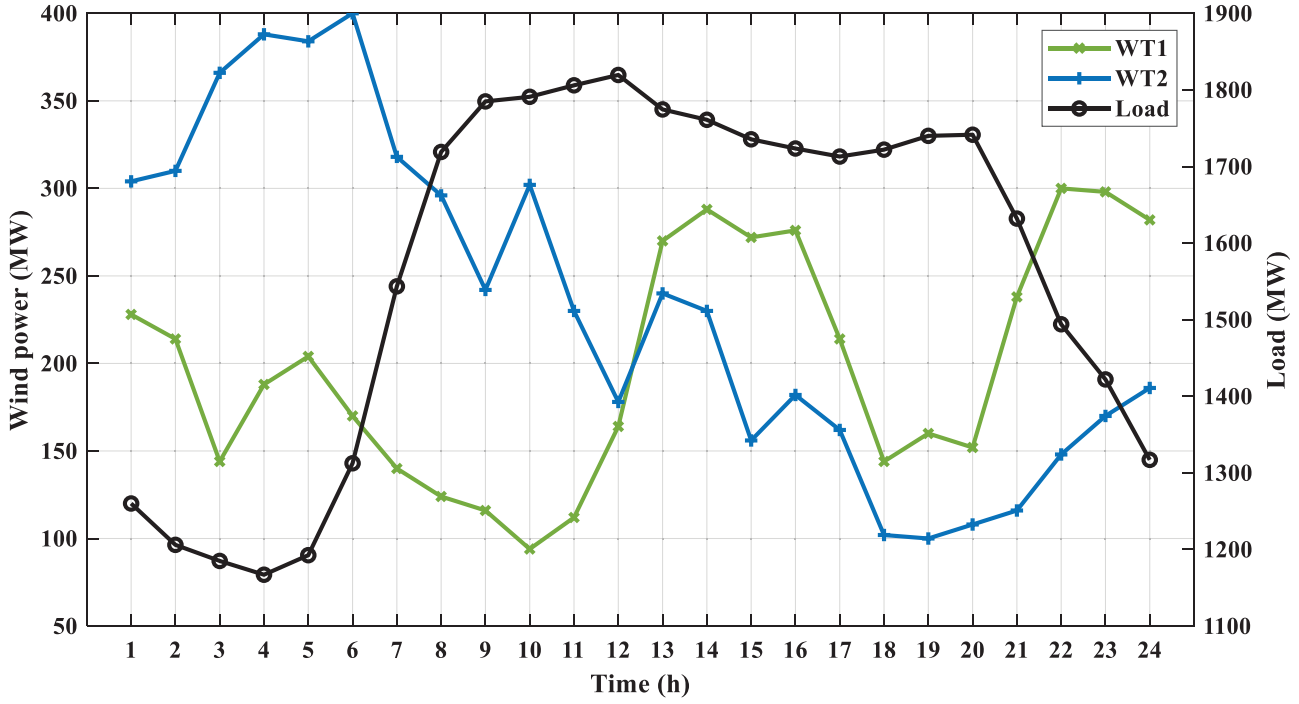

FIGURE 5 System daily load curve and forecasted production of wind farms

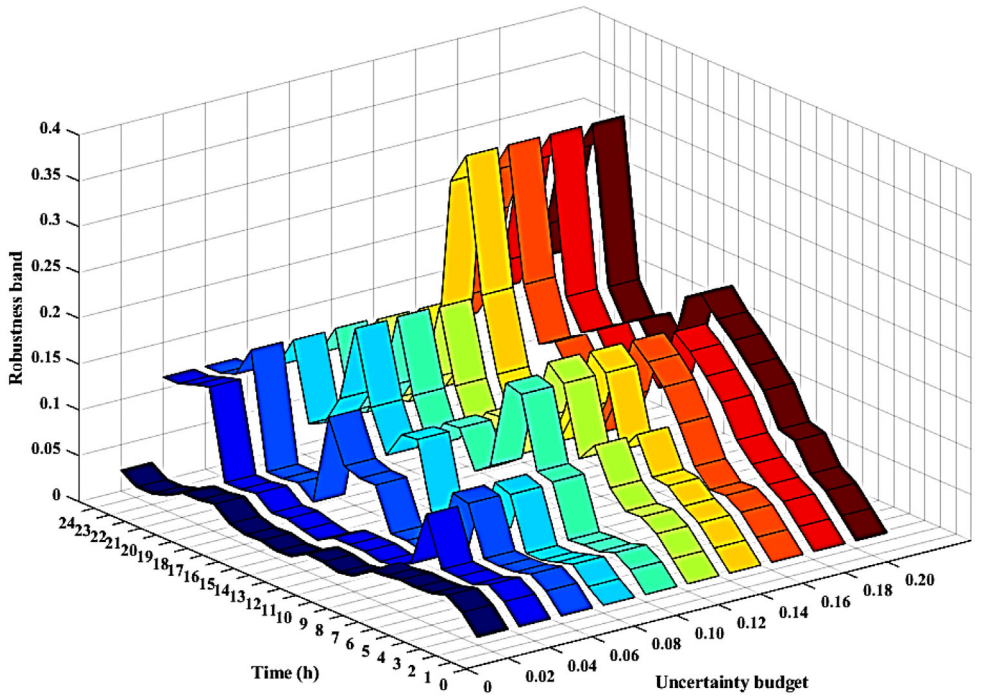

FIGURE 6 The variation of wind power robustness bands versus uncertainty budget at each time interval

The parameters of (33) and (34) are also shown in Table 1. The SOC of the VRFB is kept between the permissible ranges by (38):

$$SOC^{\min}(b) \leq SOC(b,t) \leq SOC^{\max}(b) \quad (38)$$

In the proposed model, the VRFBs participate in providing PFR in the primary stage to reduce disturbance. Indeed, due to the fast response of VRFBs and to avoid the frequent charging and discharging of them, a frequency dead-band is considered. Accordingly, the VRFBs are discharged in the power shortage

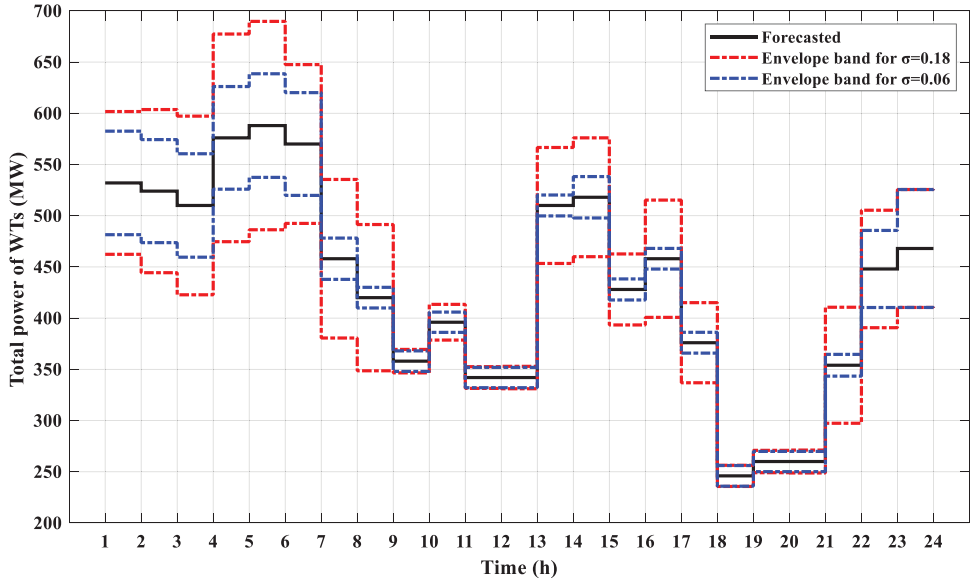

FIGURE 7 Forecasted value of total wind power generation and optimal envelope bands for uncertainty budgets of 0.18 and 0.06

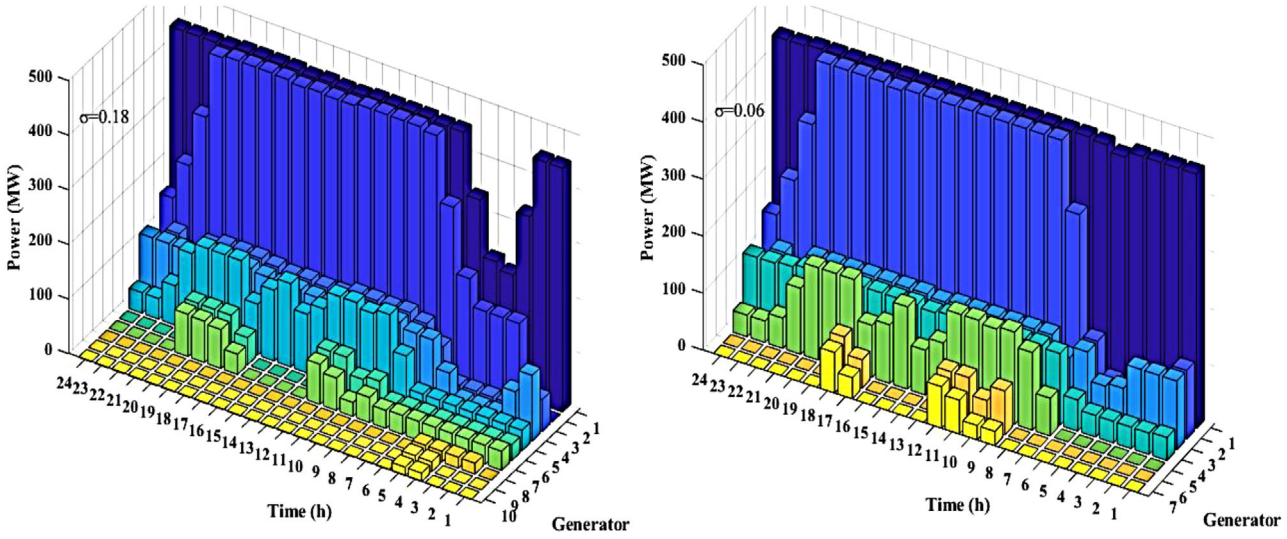

FIGURE 8 Scheduled power of SGs for uncertainty budgets of 0.18 and 0.06

$(\Delta f < \Delta f_{db})$ and charged in the power abundance $\Delta f > \Delta f_{db}$:

$$\Delta P_{VRFB}(b,t) = \begin{cases} P_c^{\max}(b,t) + P_{VRB}^d(b,t) - P_{VRB}^c(b,t) & \Delta f(t) > \Delta f_{db} \\ -\left(P_d^{\max}(b,t) - P_{VRB}^d(b,t) + P_{VRB}^c(b,t)\right) & \Delta f(t) < -\Delta f_{db} \end{cases} \tag{39}$$

Therefore, the disturbance can be modified as following:

$$\Delta P_d(t) = -\left(\sum_{j=1}^{NW} \Delta PW(j,t) - \sum_{b=1}^{NV} \Delta P_{VRFB}(b,t)\right) \tag{40}$$

The lifecycle depreciation cost of VRFB which is due to its cycle degradation can be denoted as following [12]:

$$C^B(b) = \frac{CAP(b)}{E^{rated}(b)\, LC(b)} \tag{41}$$

2.3.5 | Frequency security constraints

To avoid triggering of RoCoF relays, the following constraint should be considered:

$$-RoCoF^{\max} \le \frac{-\Delta P_d(t).f_0}{2H_{sys}(t).S_{B,sys}} \le RoCoF^{\max} \tag{42}$$

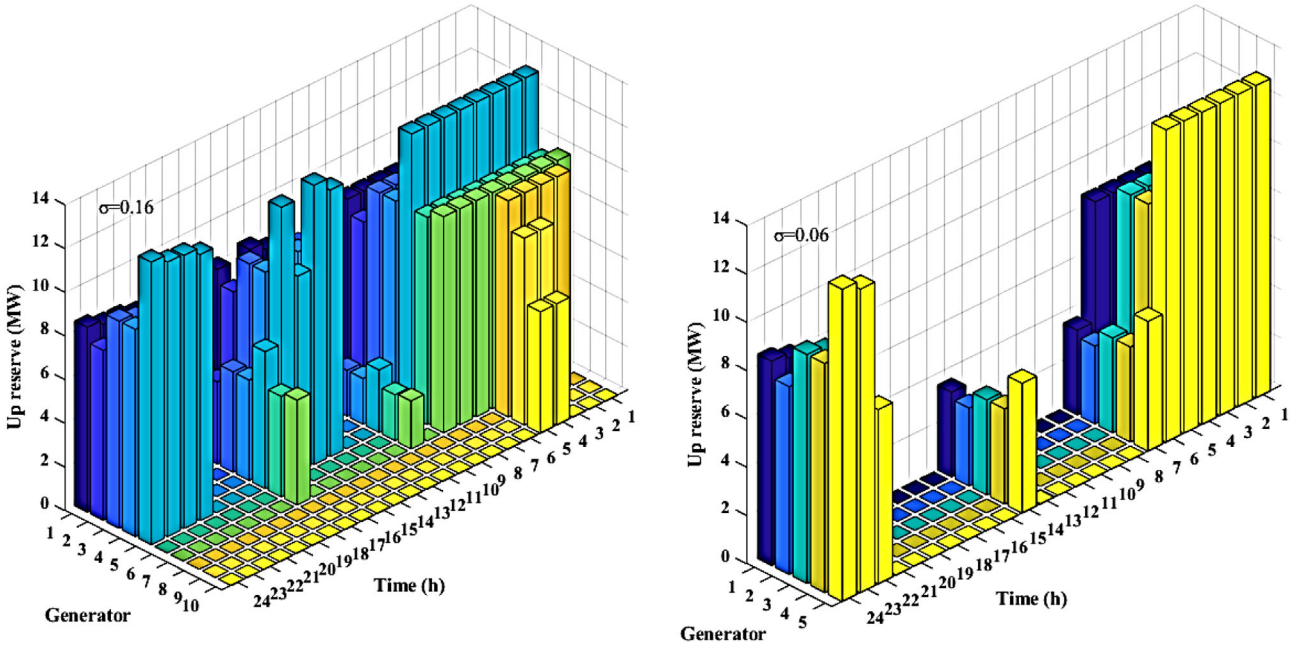

FIGURE 9 Scheduled upward reserves of SGs for uncertainty budgets of 0.18 and 0.06

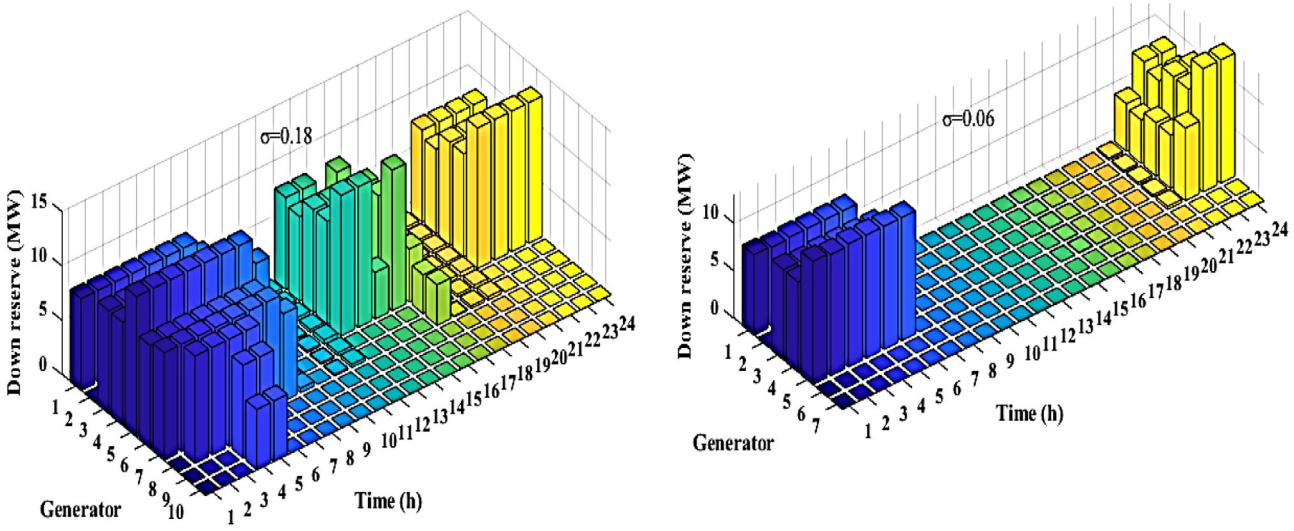

FIGURE 10 Scheduled downward reserves of SGs for uncertainty budgets of 0.18 and 0.06

To avoid under frequency relays to be triggered, the governors of SGs must response fast enough to stop frequency dropping before maximum nadir time which can be expressed based on (5–7) as following:

$$t_{\text{nadir}}^{\max}(t) \le \frac{4H_{sys}(t)\,S_{B,sys}\left(f_0 - \Delta f_{db} - f_{UF}\right)}{f_0.\Delta P_d(t)} + \frac{2H_{sys}(t)\,S_{B,sys}\Delta f_{db}}{f_0.\Delta P_d(t)} \tag{43}$$

Therefore, according to (8–10) the maximum ramp up reserve which can be delivered by SGs in the primary frequency control is as following:

$$RG^{up}(i,t) \le R_p(i)\left[\frac{4H_{sys}(t)\,S_{B,sys}\left(f_0 - \Delta f_{db} - f_{UF}\right)}{f_0.\Delta P_d(t)} + \frac{2H_{sys}(t)\,S_{B,sys}\Delta f_{db}}{f_0.\Delta P_d(t)}\right] \tag{44}$$

Similarly, the maximum ramp down reserve which can be delivered by SGs in the primary frequency control to avoid

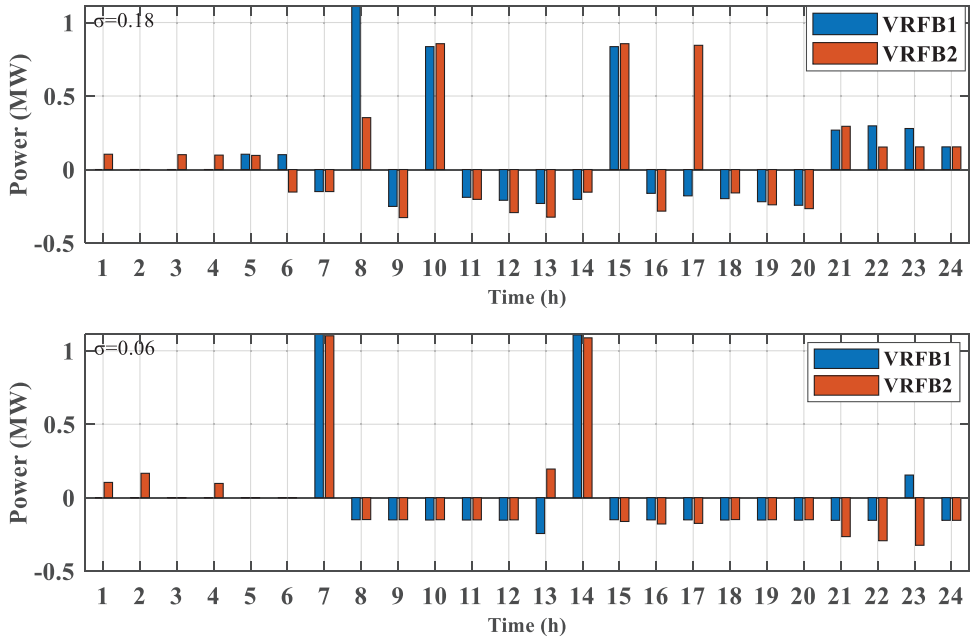

FIGURE 11 Scheduled power of VRFBs for uncertainty budgets of 0.18 and 0.06

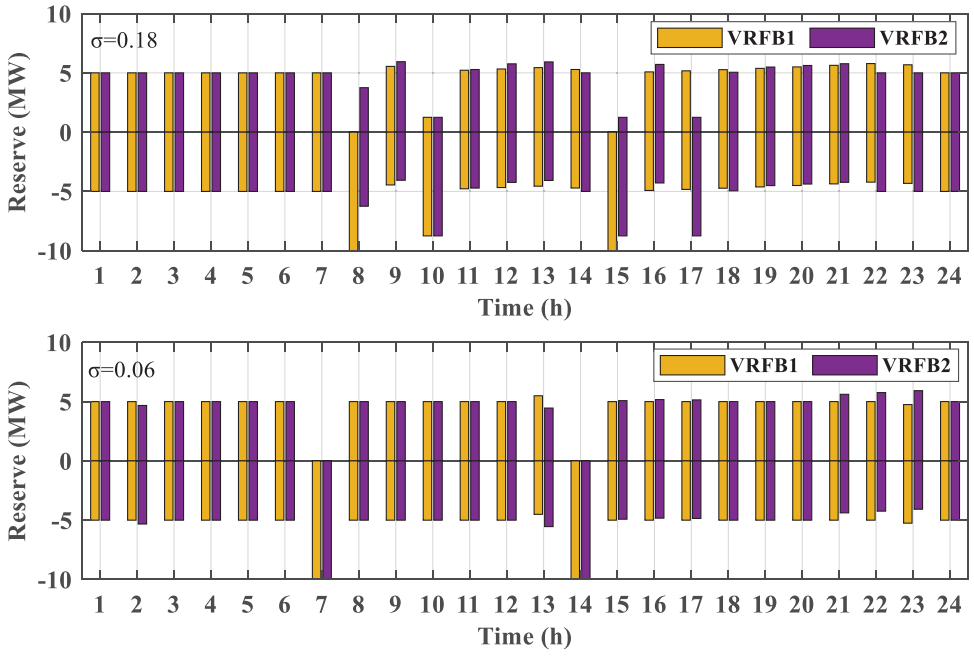

FIGURE 12 Scheduled reserves of VRFBs for uncertainty budgets of 0.18 and 0.06

triggering of over frequency relays is as following:

$$RG^{dn}(i,t) \le -R_p(i)\left[\frac{4H_{sys}(t)\,S_{B,sys}\left(f_0+\Delta f_{db}-f_{OF}\right)}{f_0.\Delta P_d(t)}+\frac{2H_{sys}(t)\,S_{B,sys}\Delta f_{db}}{f_0.\Delta P_d(t)}\right] \tag{45}$$

To preserve the steady-state frequency of system within a secure range, the following constraints have been considered:

$$\frac{\Delta P_d(t)-\sum_i RG^{up}(i,t)}{D} \le fss^{\max} \tag{46}$$

$$\frac{\Delta P_d(t)+\sum_i RG^{dn}(i,t)}{D} \le fss^{\max} \tag{47}$$

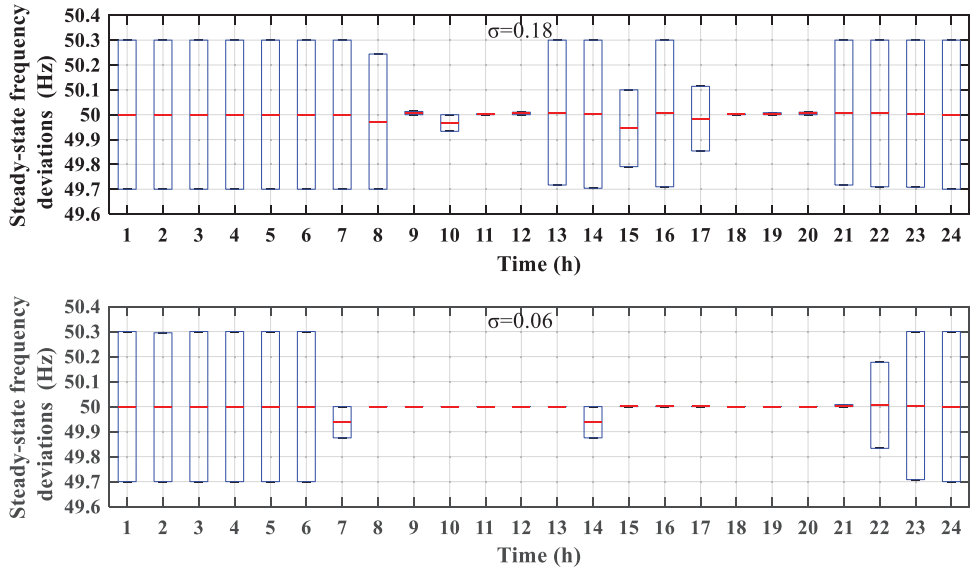

FIGURE 13 Steady-state frequency deviations for uncertainty budgets of 0.18 and 0.06

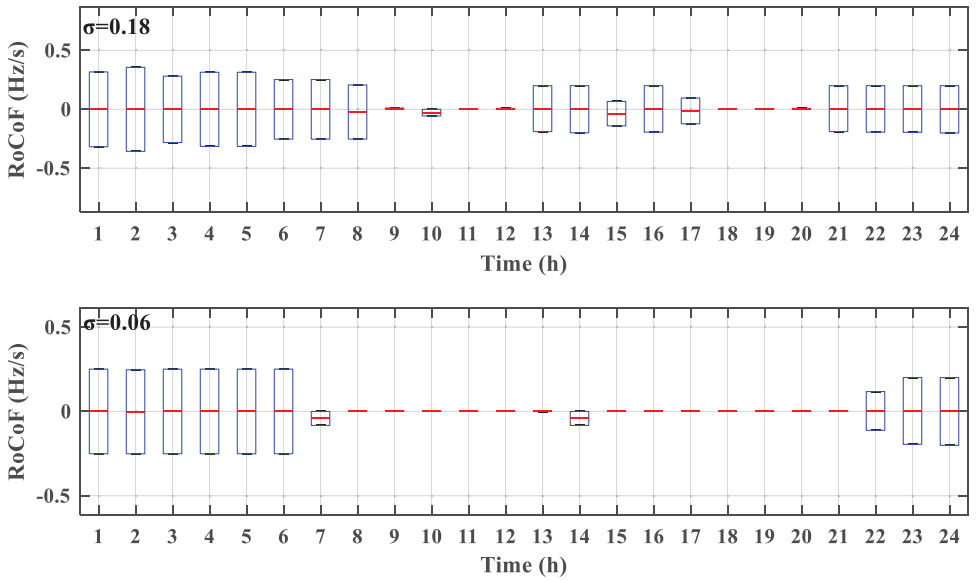

FIGURE 14 RoCoF for uncertainty budgets of 0.18 and 0.06

FIGURE 15 Frequency nadir (negative values) and frequency zenith (positive values) for uncertainty budgets of 0.18 and 0.06

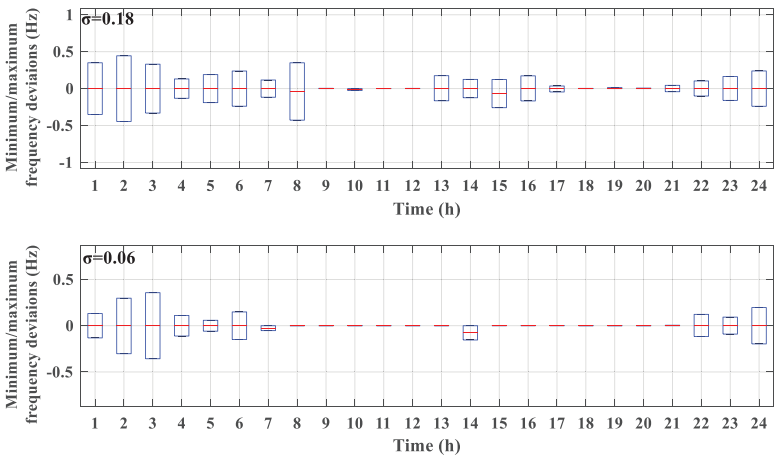

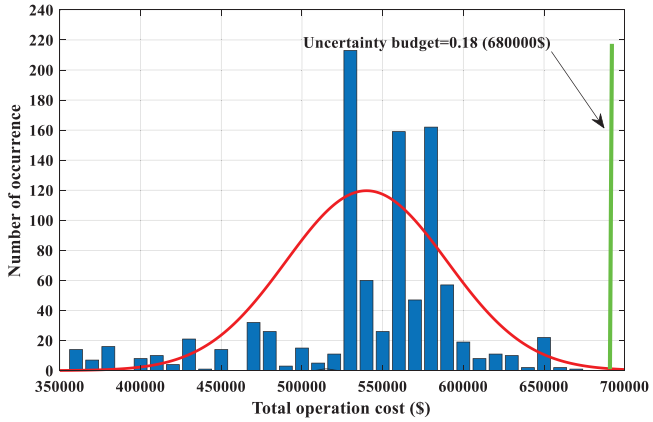

FIGURE 16 Total operation cost of system using MCS and proposed AIGDT model for uncertainty budget of 0.18

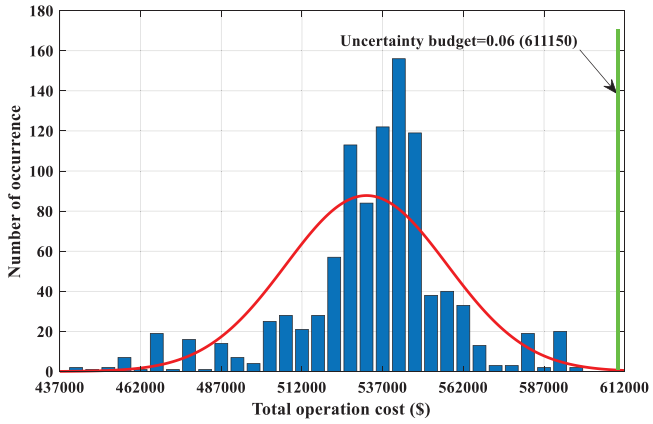

FIGURE 17 Total operation cost of system using MCS and proposed AIGDT model for uncertainty budget of 0.06

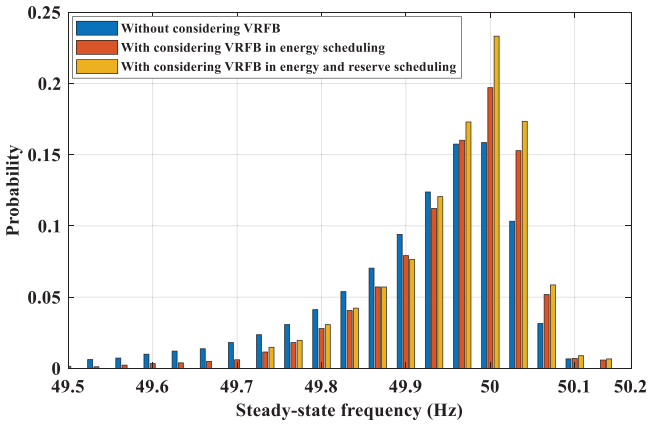

FIGURE 18 Statistical distribution of steady-state frequency for uncertainty budget of 0.18

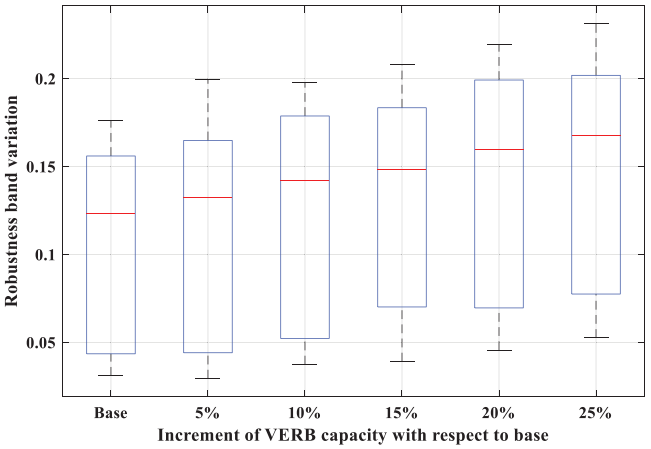

FIGURE 19 The effect of VRFBs' capacity on the uncertainties of WTs' power generation

3 | AIGDT-BASED MODEL FOR ENERGY AND RESERVE SCHEDULING MODEL

In this section the deterministic energy and reserve scheduling model which was presented in the previous section is recast based on the AIGDT approach to consider the uncertainties of WTs' power generation.

3.1 | AIGDT approach

The IGDT is a non-probabilistic approach that finds robust optimal solutions under uncertainties. In this approach, no assumption is required on the probability density function of uncertain variables which makes it effective in optimization problems with high uncertainty level. Indeed, IGDT approach finds the robustness bounds for each uncertain variable regarding an uncertainty budget which limits the objective function of the deterministic optimization problem. There are several techniques to model uncertain variables in the IGDT approach which among them the envelope band is used here to model uncertainties of WTs' power generation [19]:

$$RR\left(\gamma, \widetilde{PW}(j,t)\right) = \{\widetilde{PW}(j,t)| - \gamma \leq \frac{\widetilde{PW}(j,t) - PW(j,t)}{PW(j,t)} \leq \gamma\}; \gamma \geq 0 \quad (48)$$

As indicated in (49), the radius of envelope-band, i.e., γ, is constant during the whole scheduling horizon which compromises the frequency security of system at hours with respectively high generation of WTs. The reason is that during the hours in which the generation of WTs is high or load demand is low, the numbers of committed SGs are decreased and therefore, total inertia of system is reduced which results in more frequency variations. Likewise, the higher generation of WTs increases the forecasted uncertainty which also results in more frequency variations.

In this paper, an AIGDT approach is applied to model uncertainties in which the radius of envelope band is dynamically

updated in every scheduling horizon based on the penetration level of WTs as following:

$$RR\left(\gamma(t), \widetilde{PW(j,t)}\right) = \{\widetilde{PW(j,t)} | -\gamma(t) \leq \frac{\widetilde{PW(j,t)} - PW(j,t)}{PW(j,t)} \leq \gamma(t)\};\ \gamma(t) \geq 0\ ,\ \forall j, \forall t; \tag{49}$$

The objective function is defined, to maximize the robustness, i.e., the envelope bands of power generation from WTs, while a target operation cost of deterministic problem is guaranteed for the risk-averse operator. In this way, the uncertainty modelling and optimization are performed simultaneously:

$$\Gamma(DV_1, DV_2, Cost) = \max_{DV_1} \left\{ \sum_{t=1}^{N_T} \omega(t)\gamma(t) \mid \max_{DV_2} Cost\left(DV_1, \widetilde{PW(j,t)}\right) \leq Cost^{det} \times (1+\sigma) \right\} \tag{50}$$

where $DV_1 = \{\gamma, u, v, PG, w, RG^{up}, RG^{dn}, PB^{cba}, PB^{dis}\}$ and $DV_2 = \{\widetilde{PW}\}$. As mentioned, the radius of envelope bands should be enlarged during the hours in which the generation of WTs is respectively high and vice versa. Accordingly, total inertia of the system is increased and therefore, frequency security is enhanced. To this end, the weighted factors in the objective function are defined as following:

$$\omega(t) = \frac{\sum_{j=1}^{NW} PW(j,t)}{\sum_{n=1}^{NB} Load(n,t) - \sum_{j=1}^{NW} PW(j,t)} \tag{51}$$

The AIGDT-based model in (50) and (51) is a bi-level problem which is presented in the next sub-section.

3.2 | Bi-level AIGDT-based model

The bi-level AIGDT-based model can be formulated as following:

$$\max_{DV_1} \sum_{t=1}^{N_T} \omega(t)\gamma(t) \tag{52}$$

subject to

$$Cost \leq Cost^{det} \times (1+\sigma) \tag{53}$$

(13–48)

$$Cost = \max_{P\tilde{W}(j,t)} \sum_{t=1}^{N_T}\sum_{i=1}^{N_I} \left(C^{SD}(i,t)\,v(i,t) + C^{SU}(i,t)\,w(i,t) + C^{F}(i,t)\,u(i,t) + C^{V}(i)\,PG(i,t) + C^{up}(i)\,RG^{up}(i,t) + C^{dn}(i)\,RG^{dn}(i,t)\right) + \sum_{t=1}^{N_T}\sum_{b=1}^{N_B} C^{B}(b)\left(PB^{cba}(b,t) + PB^{dis}(b,t)\right) + \sum_{t=1}^{N_T}\sum_{n=1}^{N_B} C^{ENS}(t)\,ENS(n,t) + \sum_{t=1}^{N_T}\sum_{n=1}^{NB} C^{EWS}(t)\,EWS(n,t) \tag{54}$$

subject to

$$-\gamma(t) \leq \frac{\widetilde{PW}(j,t) - PW(j,t)}{PW(j,t)} \leq \gamma(t); \quad \gamma(t) \geq 0 \tag{55}$$

In the first level, the optimal energy and reserve scheduling is determined to maximize the robustness, i.e., radius of envelope-bands, while ensuring that the target operation cost is achieved. The second level calculates the worst realization of operation cost which occurs due to uncertainty of generation power from WTs. The bi-level optimization problems cannot be solved directly via commercial software. In this paper, the developed bi-level optimization problem is recast into an equivalent single-level optimization problem using the duality theory which is represented in the reminder of this section.

3.3 | Equivalent single-level AIGDT-based model

To preserve the frequency security of the power system during scheduling horizon optimal amount of upward and downward reserves should be scheduled to compensate uncertainties in power generation from WTs. Otherwise, mandatory load shedding and wind power spillage is inevitable which increases total operation cost of power system, significantly. More in details, if the power generation of WTs is reduced (increased) and scheduled upward (downward) reserves are low, the frequency of power system is reduced (increased) from the nominal and the load shedding (wind power spillage) is inevitable to preserve the frequency security. Likewise, the line flow constraints may not lead to dispatch of scheduled reserves and therefore, it is necessary to perform load shedding and wind power spillage. Let us represent $\widetilde{PW(j,t)}$ as following:

$$\widetilde{PW(j,t)} = \mu(j,t)\,PW^{\min}(j,t) + (1-\mu(j,t))\,PW^{\max}(j,t);\ 0 \leq \mu(j,t) \leq 1 \tag{56}$$

Note that based on (55), the maximum and minimum power generations from the WTs occur in the upper and lower of envelope bands, respectively. These facts can be described mathematically as following:

$$PW^{max}(j,t) = (1+\gamma(t)) \times PW(j,t) \tag{57}$$

$$PW^{min}(j,t) = (1-\gamma(t)) \times PW(j,t) \tag{58}$$

Accordingly, power balance and transmission line capacity constraints can be represented as following:

$$\begin{aligned}
&\sum_{i=1}^{NG} PG(i,t) \\
&+\sum_{j=1}^{NW} \left(\mu(j,t)\, PW^{\min}(j,t) + (1-\mu(j,t))\, PW^{\max}(j,t)\right) \\
&+\sum_{b=1}^{NV} \left(P^{d}_{VRB}(b,t) - P^{c}_{VRB}(b,t)\right) = \sum_{n=1}^{NB} Load(n,t)
\end{aligned} \tag{59}$$

$$\begin{aligned}
-F^{\max}(l) \le &\sum_{n=1}^{NB} K(l,n) \Bigg(\sum_{i\in\Omega_n^G} PG(i,t) \\
&+ \sum_{j\in\Omega_n^W} \left(\mu(j,t)\, PW^{\min}(j,t) + (1-\mu(j,t))\, PW^{\max}(j,t)\right) \\
&+ \sum_{b\in\Omega_n^B} \left(P^{d}_{VRB}(b,t) - P^{c}_{VRB}(b,t)\right) - Load(n,t) \Bigg) \le F^{\max}(l)
\end{aligned} \tag{60}$$

Constraints (59) and (60) are violated if optimal amount of upward and downward reserves is not scheduled. Accordingly, the frequency security of the power system should be preserved in the following worst-case scenarios.

The worst-case scenario for the upward reserve is as following:

$$\begin{cases}
\delta^{up}(t) = \min\limits_{\mu^1(j,t)} \left(\begin{array}{c} \sum\limits_{i=1}^{NG} PG(i,t) + \\ \sum\limits_{j=1}^{NW} \left(\mu^1(j,t)\, PW^{min}(j,t) + \left(1-\mu^1(j,t)\right) PW^{max}(j,t)\right) \\ + \sum\limits_{b=1}^{NV} \left(P^{d}_{VRB}(b,t) - P^{c}_{VRB}(b,t)\right) - \sum\limits_{n=1}^{NB} Load(n,t) \end{array} \right) \ge 0 \\
s.t. \quad 0 \le \mu^1(j,t) \le 1
\end{cases} \tag{61}$$

where δ^{up} is the minimum upward reserve which should be greater than or equal to zero to avoid load shedding, i.e., $\sum_{t=1}^{NT}\sum_{n=1}^{NB} ENS(n,t) = 0$. To recast a single-level optimization problem, the duality theory can be applied to consider the worst-case scenario for the upward reserve [31]:

$$\begin{cases}
\begin{array}{c} \sum\limits_{i=1}^{NG} PG(i,t) + \sum\limits_{j=1}^{NW} PW^{\max}(j,t) - \sum\limits_{j=1}^{NW} \varphi(j,t) \\ + \sum\limits_{b=1}^{NV} \left(P^{d}_{VRB}(b,t) - P^{c}_{VRB}(b,t)\right) \ge \sum\limits_{n=1}^{NB} Load(n,t) \end{array} \\
s.t. \quad -\varphi(j,t) \le \left(PW^{\min}(j,t) - PW^{\max}(j,t)\right), \varphi(j,t) \ge 0
\end{cases} \tag{62}$$

Similarly, the worst-case scenario for the downward reserve as well as positive and negative power flow can be obtained as following:

$$\begin{cases}
\begin{array}{c} \sum\limits_{i=1}^{NG} PG(i,t) + \sum\limits_{j=1}^{NW} PW^{max}(j,t) + \sum\limits_{j=1}^{NW} \psi(j,t) \\ + \sum\limits_{b=1}^{NV} \left(P^{d}_{VRB}(b,t) - P^{c}_{VRB}(b,t)\right) \le \sum\limits_{n=1}^{NB} Load(n,t) \end{array} \\
s.t. \quad \psi(j,t) \ge \left(PW^{min}(j,t) - PW^{max}(j,t)\right), \psi(j,t) \ge 0
\end{cases} \tag{63}$$

$$\begin{cases}
\begin{array}{c} \sum\limits_{i=1}^{NG} K(l,i)\, PG(i,t) - \sum\limits_{n=1}^{NB} K(l,n)\, Load(n,t) + \sum\limits_{j=1}^{NW} \lambda(j,t) + \\ \sum\limits_{j=1}^{NW} K(l,j)\, PW^{max}(j,t) \sum\limits_{b=1}^{NV} K(l,b) \left(P^{d}_{VRB}(b,t) - P^{c}_{VRB}(b,t)\right) \le F^{max}(l) \end{array} \\
s.t. \quad -\lambda(j,t) \le \left(PW^{min}(j,t) - PW^{max}(j,t)\right), \lambda(j,t) \ge 0
\end{cases} \tag{64}$$

$$\begin{cases}
\begin{array}{c} \sum\limits_{i=1}^{NG} K(l,i)\, PG(i,t) - \sum\limits_{n=1}^{NB} K(l,n)\, Load(n,t) - \sum\limits_{j=1}^{NW} \xi(j,t) + \\ \sum\limits_{j=1}^{NW} K(l,j)\, PW^{min}(j,t) \sum\limits_{b=1}^{NV} K(l,b) \left(P^{d}_{VRB}(b,t) - P^{c}_{VRB}(b,t)\right) \ge -F^{max}(l) \end{array} \\
s.t. \quad \xi(j,t) \ge \left(PW^{min}(j,t) - PW^{max}(j,t)\right), \xi(j,t) \ge 0
\end{cases} \tag{65}$$

Finally, the proposed single-level AIGDT-based model can be derived as follows:

$$\begin{cases}
\begin{array}{c} \sum\limits_{i=1}^{NG} K(l,i) PG(i,t) - \sum\limits_{n=1}^{NB} K(l,n)\, Load(n,t) \sum\limits_{j=1}^{NW} \zeta(j,t) \\ + \sum\limits_{j=1}^{NW} K(l,j) PW^{\min}(j,t) \sum\limits_{b=1}^{NV} K(l,b) \left(P^{d}_{VRB}(b,t)\right) \ge -F^{\max}(l) \end{array} \\
s.t. \quad \zeta(j,t) \ge (PW^{\min}(j,t) - PW^{\max}(j,t)), \zeta(j,t) \ge 0
\end{cases} \tag{66}$$

subject to

$$Max_{DV_1} \sum_{t=1}^{N_T} \omega(t)\gamma(t) \tag{67}$$

$$Cost \le Cost^{det} \times (1+\sigma) \tag{68}$$

$$\begin{aligned} Cost = & \sum_{t=1}^{N_T}\sum_{i=1}^{N_I}\left(C^{SD}(i,t)v(i,t) + C^{SU}(i,t)w(i,t)\right. \\ & + C^{F}(i,t)u(i,t) + C^{V}(i)PG(i,t) + C^{up}(i) \end{aligned} \tag{69}$$

$$\begin{aligned} & RG^{up}(i,t) + C^{dn}(i)RG^{dn}(i,t)\Big) + \sum_{t=1}^{N_T}\sum_{b=1}^{N_B} C^{B}(b)\left(P^{d}_{VRB}(b,t)\right. \\ & \left. + P^{c}_{VRB}(b,t)\right) + \sum_{t=1}^{N_T}\sum_{n=1}^{NB} C^{ENS}(t)\,ENS(n,t) \\ & + \sum_{t=1}^{N_T}\sum_{n=1}^{NB} C^{EWS}(t)\,EWS(n,t) \end{aligned} \tag{70}$$

(13–48), (51), (56), (57), (58), (62), (63), (64), and (65)

4 | NUMERICAL RESULTS

To have a general overview of the applied BMS and SCADA system in this case study to communicate between two VRFB units for both energy and reserve scheduling, a short description of monitoring system is added as follows. In general, for grid-scale BESS, the BMS and SCADA system is highly recommended [32]. Continuously monitoring and control of the BESS conditions such as voltage, temperature, current, and SoC is crucial for a safe operation of BESS [33]. Overcharging, overtemperature, and mechanical abuse are the most important safety events to address [34]. These tasks are fulfilled by the BMS, the inverter control unit, and the SCADA system. A SCADA system for BESS needs to coordinate the data from the BMS, and the power conversion system (PCS) (includes DC power, inverters, and transformer) [35].

In this case study, the real-time monitoring system consists of four main parts, first, the BMS which guarantee the proper operation of each VRFB unit, second, the PCS (mostly is used to control the inverters and other power electronic components for safe operation), then the SCADA system to communicate between different parts and, finally the database server or any hardware for monitoring purposes. The BMS which is the main part of the proposed system monitors measurements and makes sure that the VRBFs are operated within the safe operations. As long as the SCADA system receives a request from measured signals of the VRBFs regarding the energy and reserve scheduling, it will dispatch the power between the individual VRBFs strings. This dispatch is the task of the optimal energy management system for each VRBFs string. As it can be seen in Figure 4, the BMS and SCADA system for communication of the VRFBs are considered with green and blue dashed lines, respectively.

4.1 | Data

This section presents numerical results obtained from implementing the proposed model on a modified IEEE 39 bus test system which is shown in Figure 4. The specifications of transmission lines and bus loads can be found in [36]. The technical and economic data of SGs are given in Table 2 [37].

System daily load curve and the forecasted production of wind farms are retrieved from [21] and shown in Figure 5. It should be noted that the maximum penetration level of WTs is considered 20% of the total capacity of SGs. The parameters of VRFBs are presented in Table 3 [12]. It is assumed that maximum 10% of VRFBs' capacity is used to provide reserves. The values of $f_0 = 50$ Hz, $RoCoF^{max} = 0.75$ Hz/s, $D = 2\%$, and $\Delta f^{ss} = 0.3$ Hz, $f^{zenith} = 0.5$ Hz, and $f^{nadir} = -0.5$ Hz are selected as per National Grid Standards [3]. The scheduling horizon is 24 hours on an hourly basis.

The optimization problem is programed in the generalized algebraic modelling systems (GAMS) environment and solved by DICOPT solver. A personal computer with Core i5 CPU and 4GB RAM was used with optimality gap equal to 1×10^{-4}.

4.2 | Results

The variation of wind power robustness band in response to increasing changes of uncertainty budget is shown in Figure 6. As in the proposed model, the robustness bands are adaptive, it can be seen, with increasing the uncertainty budget from 0.02 to 0.2, the robustness band is increased which means the frequency security of system can be preserved following more severe fluctuations in the generation of WTs, but with the trade-off of higher operation cost. However, for values of uncertainty budget which are greater than 0.2, the frequency security of the system cannot be preserved which indicates the upper robustness limit of system against fluctuations in the generation of WTs. On the other hand, during the hours in which the generation of WTs is high (e.g., hours 1 to 5) or load demand is low (e.g., hours 22 to 24), the robustness band is increased which leads to more scheduled reserve to preserve frequency security of system. The reason is that during these hours the numbers of committed SGs are decreased and therefore, total inertia of system is reduced which results in more frequency deviations.

Forecasted value of total wind power generation and optimal envelope bands for uncertainty budgets of 0.18 and 0.06 are shown in Figure 7. As can be seen, during high generation of WTs the envelope bands are increased. Since higher share of WTs in the generation increases the forecasted uncertainty and resulting frequency deviations, therefore, a larger envelope band can guarantee the frequency security of the system against wind power uncertainty. Likewise, with increasing the uncertainty budget, the envelope band is enlarged which means that the higher wind power uncertainty can be handled while the frequency security of the system is preserved. Indeed, with increasing the uncertainty budget the operator can schedule more upward and downward reserves to compensate wind

TABLE 2 The technical and economic data of SGs

	G1	G2	G3	G4	G5	G6	G7	G8	G9	G10
PG^{max} (MW)	455	455	130	130	162	80	85	55	55	55
PG^{min} (MW)	150	150	20	20	25	20	25	10	10	10
C^F ($/MWh)	16.19	17.26	16.60	16.5	19.7	22.26	22.74	25.92	27.27	27.79
C^V ($/h)	1000	970	700	680	450	370	480	660	665	670
C^{SU} ($)	9000	10,000	1100	1120	1800	349	520	60	60	60
C^{SU} ($)	9000	10,000	1100	1120	1800	349	520	60	60	60
RC^{up}/RC^{dn} ($)	32	34	33	33	40	44	45	52	54	55
RU^{up}/RU^{dn} (MW/h)	120	120	60	50	70	30	34	22	20	10
$\frac{T^{up}}{T^{dn}}$ (h)	6	6	5	5	5	4	4	1	1	1
R_G (%)	3.54	3.85	3.16	3.16	2.31	3.16	3.03	3.03	3.50	5.39
H (s)	5	4.33	4.48	3.58	4.33	4.35	3.77	3.47	3.45	4.20

TABLE 3 The technical data of VRFBs

	SOC^{min}	SOC^{min}	P_c^{max} (MW)	P_d^{max} (MW)	E^{rated} (MWh)	LC	CAP ($/kW)	CAP ($/kWh)
VRFB	0.95	0.05	5	5	50	12,000	600	150

power uncertainty which improves the frequency security of the system.

Results of power scheduling for uncertainty budgets of 0.18 and 0.06 are shown in Figure 8. As can be seen, the cheapest SGs (e.g., 1 and 2) are dispatched more to reduce the operation cost of the system. However, with increasing the uncertainty budget, more reserves should be provided by SGs and therefore, scheduled power of cheapest SGs is reduced. On the other hand, a greater number of SGs should be committed which also increases the operation cost of the system. This cost should be paid to preserve the frequency security of system against fluctuations generated power of WTs.

The results of the upward and downward scheduled reserves for uncertainty budgets of 0.18 and 0.06 are shown in Figures 9 and 10, respectively. As can be seen, during high generation of WTs more reserves are scheduled to preserve the frequency security of the system. Likewise, the SGs with larger droop (e.g., SG 5) are used more to provide reserve due to their faster response. With increasing the uncertainty budget, the scheduled reserves are increased to compensate uncertainty of power generation from WTs and therefore, a greater number of SGs should be committed which increases the operation cost of system.

The scheduled power and reserves of VRFBs are shown in Figures 11 and 12, respectively. As can be seen, the VRFBs are mainly scheduled to provide up and down reserves. This is due to the fast response of VRFBs which indicates their noteworthy role in compensating uncertainty of WTs' power. This strategy releases the capacity of SGs to provide more reserves which increases the frequency security and decreases the operating cost.

The steady-state frequency deviations and RoCoF for uncertainty budgets of 0.18 and 0.06 are shown in Figures 13 and 14, respectively. As can be seen, during high power generation of WTs the frequency deviations and RoCoF are large which is due to the higher uncertainty. However, the frequency deviations and its RoCoF are suitably managed within secure range and therefore, the frequency security of the system is totally preserved. Likewise, with increasing the uncertainty budget, the frequency deviations and its RoCoF are increased. The reason is that optimal envelope band is increased and therefore, more wind power uncertainty can be handled by scheduled reserves regarding frequency security.

The values of frequency nadir and zenith for uncertainty budgets of 0.18 and 0.06 are shown in Figure 15. As can be seen, the frequency is preserved within the secure range using the scheduled reserves. It should be mentioned that during hours in which frequency is zero, the uncertainty in power generation of WTs is totally compensated by VRFBs and therefore, the frequency of system can be fixed to the nominal values.

To evaluate the robustness of the proposed AIGDT-based model, the Monte Carlo simulation (MCS) is used. To this end, 1000 random scenarios of power generation from WTs are generated and reduced in a way that Equation (58) is satisfied. Then total operation cost of system is calculated by solving (12–48) for each scenario. Figures 16 and 17 show the results using MCS and proposed AIGDT model for uncertainty budgets of 0.18 and 0.06, respectively. As can be seen, the operation cost of system is always lower than the specified value which is obtained from the proposed AIGDT model (vertical green line). Therefore, it is confirmed that using the proposed AIGDT model the operation cost will be lower than the target value of $(Cost^{det} \times (1 + \sigma))$ while the frequency security of the system is preserved. Likewise, the results indicate that with increasing the uncertainty budget, the variation of total operation cost is intensified. The reason is that the wind power robustness band

is increased and therefore, the larger deviations of wind power from forecasted are possible which impose more scheduled reserves with higher operation cost.

Statistical distribution of steady-state frequency for uncertainty budgets of 0.18 is shown in Figure 18. As can be seen, without considering VRFBs the peak of steady-state frequency is shifted to low frequency and therefore, the frequency stability is reduced. Likewise, when VRFBs are incorporated in the energy and reserve scheduling, the statistical distribution of steady-state frequency is shifted to the right side which means improvement of frequency stability of system, with considering VRFBs in energy and reserve scheduling, the distribution of steady-state frequency is preserved in the secure range and the frequency stability of the system is guaranteed.

In Figure 19, the effect of VRFBs' capacity on the robustness band is investigated for uncertainty budget of 0.18. The results indicate that the robustness bands are increased with increasing the capacity of VRFBs. Indeed, more uncertainties associated with power generation of WTs can be managed regarding the frequency security of system. The reason is that more fast reserves are provided by the VRFBs. Therefore, the optimal size of VRFBs considering techno-economic constraints of systems is important which can be studied in future work. Likewise, the operation cost of the system is reduced. Since, not only the capacity of SGs becomes free to schedule energy with lower cost, but also the expensive SGs are not required to commit.

5 | CONCLUSION

The growing integration of wind turbines in power systems leads to frequency security challenges for operators. To address this issue, in this paper a novel energy and reserve scheduling model which takes the benefit of a real-time monitoring system based on a SCADA system for power systems is proposed. In the proposed model, VRFBs can be scheduled in both energy and reserve. The uncertainties of WTs' power are considered by an AIGDT approach in which the robustness band is dynamically changed in every scheduling horizon based on the extent of uncertainties. The numerical results indicate that using the proposed model, the static and dynamic security of the power system is assured by preserving the frequency nadir, rate of change of frequency, and quasi-steady-state frequency in the predefined range and by an increment of 6% in the operation cost, the optimal solution is robust against 15% of uncertainty in the wind output power. It was found that the VRFBs can optimally participate in primary frequency control of the power system by providing reserve in the primary frequency interval. Therefore, they can be considered one of the actors in the primary frequency response of the power system. The future extension of this research work will involve the development of a comprehensive model for optimal sizing of VRFBs.

CONFLICT OF INTEREST STATEMENT

The authors have declared no conflict of interest.

FUNDING INFORMATION

None.

DATA AVAILABILITY STATEMENT

The data that support the findings of this study are available from the corresponding author upon reasonable request.

Indices and sets

Ω_n^B	set of VRFBs which are connected to bus n
Ω_n^G	set of SGs which are connected to bus n
Ω_n^W	set of WTs which are connected to bus n
$l \in NL$	index/set of transmission lines
$n \in NB$	index/set of busses
$t \in NT$	index/set of scheduling time
$b \in NV$	index/set of VRFBs
$i \in NG$	index/set of SGs
$j \in NW$	index/set of WTs

Parameters

C^B	lifecycle depreciation cost of VRFB
C^{ENS}	penalty of Energy not supplied
C^{EWS}	penalty of wind energy spillage
C^F/C^V	fuel cost coefficients of SG
C^{SU}/C^{SD}	start-up/shut-down cost of DG
C^{up}/C^{dn}	up/down reserve cost
$F^{\max}$	maximum capacity of transmission line
$P_{VRB}^{c,p.u}/P_{VRB}^{d,p.u}$	charge/discharge power of VRFB in $p.u$
$PW^{\min}/PW^{\max}$	maximum/minimum limit of Wind turbine generation
P_{ab}^c/P_{ab}^d	charge/discharge absorb power of VRFB
RG^{up}/RG^{dn}	scheduled up/down reserve of SG
f_0	nominal frequency of power system
f_{UF}/f_{OF}	trigger of under/over frequency relays
f_{db}	dead band of frequency trajectory
$f_{ss}^{\max}$	maximum permissible steady-state frequency
u^c/u^d	binary variable indicating charge/discharge status of VRFB
D	frequency elasticity of power system
CAP	capital investment of VRFB
H	inertia of each SG
K	generation distribution shift factor
LC	maximum life cycle of VRFB
PW	generation power of Wind turbine
u	commitment status of SG
v/w	binary variable indicating shutdown/startup status of SG
σ	uncertainty budget in IGDT approach
ω	weighted factors in OF

Symbols

$\widetilde{(\bullet)}$	uncertain form of variable $(\bullet)$
E^{rated}	rated capacity of VRFB
$PG^{\max}/PG^{\min}$	maximum/minimum power of SG
$P_c^{\max}/P_d^{\max}$	maximum charge/discharge power rate of VRFB

P_d	disturbance power due to uncertainty in generation of WTs
P_m	mechanical power of SG
RG^{up_max}/RG^{dn_max}	maximum ramp up/down capability of SG
R_G	value of SGs' droop
$RoCoF^{\max}$	maximum rate of charge of frequency
$S_{B,sys}$	base power of system
$SOC^{\min}/SOC^{\max}$	minimum/maximum state of charge of VRFB
$T^{ON/OFF}$	the number of initial periods during which the unit must be online/off-line
T_d	governor response delivery time of SGs
T^{up}/T^{dn}	minimum up/down time of SG
$Load$	load of the power system
RU/RD	ramp-up/down limit of SG
SU/SD	start-up/shut-down ramp limit of SG

Variables

PFR^{tot}	total primary frequency reserve
P^c_{VRB}/P^d_{VRB}	charge/discharge power of VRFB
δ^{up}/δ^{dn}	minimum value of upward/downward reserves
η_c/η_d	charge/discharge efficiency of VRFB
ΔP_d	change of power during disturbance
$Cost$	total operation cost of power system
ENS	expected energy not supplied
EWS	expected wind energy spillage
f	frequency of power system
PG	generation power of SG
γ	radius of envelope-band in IGDT approach
$\mu, \mu^1, \mu^2, \mu^3, \mu^4$	auxiliary variables for deriving single level AIGDT based model
$\varphi, \psi, \lambda, \zeta$	dual variables of constraints for deriving single level AIGDT based model

REFERENCES

1. Li, W., Du, P., Lu, N.: PFR ancillary service in low-inertia power system. IET Gener. Transm. Distrib. 14(5), 920–930 (2020)
2. Đaković, J., Krpan, M., Ilak, P., Baškarad, T., Kuzle, I.: Impact of wind capacity share, allocation of inertia and grid configuration on transient RoCoF: The case of the Croatian power system. Int. J. Electr. Power Energy Syst. 121, 106075 (2020)
3. Kushwaha, P., Prakash, V., Bhakar, R., Yaragatti, U.R.: PFR constrained energy storage and interruptible load scheduling under high RE penetration. IET Gener. Transm. Distrib. 14(15), 3070–3077 (2020)
4. Malekpour, M., Zare, M., Azizipanah-Abarghooee, R., Terzija, V.: Stochastic frequency constrained unit commitment incorporating virtual inertial response from variable speed wind turbines. IET Gener. Transm. Distrib. 14(22), 5193–5201 (2020)
5. Ahmadi, H., Ghasemi, H.: Security-constrained unit commitment with linearized system frequency limit constraints. IEEE Trans. Power Syst. 29(4), 1536–1545 (2014)
6. Rabbanifar, P., Amjady, N.: Frequency-constrained unit-commitment using analytical solutions for system frequency responses considering generator contingencies. IET Gener. Transm. Distrib. 14(17), 3548–3560 (2020)
7. Li, H., Lu, Z., Qiao, Y., Zhang, B.: Frequency dynamics constrained unit commitment with wind plants. In: 2020 IEEE Power & Energy Society General Meeting (PESGM), IEEE, pp. 1–5 (2020)
8. Wen, Y., Li, W., Huang, G., Liu, X.: Frequency dynamics constrained unit commitment with battery energy storage. IEEE Trans. Power Syst. 31(6), 5115–5125 (2016)
9. Pereira, F.B., Paucar, V.L., Saraiva, F.S.: Power system unit commitment incorporating wind energy and battery energy storage. In: 2018 IEEE XXV International Conference on Electronics, Electrical Engineering and Computing (INTERCON), IEEE, pp. 1–4 (2018)
10. Bruninx, K., Delarue, E.: Improved energy storage system & unit commitment scheduling. In: 2017 IEEE Manchester PowerTech, IEEE, pp. 1–6 (2017)
11. Alotto, P., Guarnieri, M., Moro, F.: Redox flow batteries for the storage of renewable energy: A review. Renew. Sustainable Energy Rev. 29, 325–335 (2014)
12. Padhee, M., Pal, A., Mishra, C., Vance, K.A.: A fixed-flexible BESS allocation scheme for transmission networks considering uncertainties. IEEE Trans. Sustainable Energy 11(3), 1883–1897 (2020)
13. Martinez, M., Molina, M.G., Mercado, P.E.: Optimal sizing and location of vanadium redox flow battery in a power system with high wind power generation. J. Eng. 2019(18), 5038–5043 (2019)
14. Xiong, B., et al.: Design of a two-stage control strategy of vanadium redox flow battery energy storage systems for grid application. IEEE Trans. Sustainable Energy 1–12 (2022)
15. Gu, F.C., Chen, H.C.: Modelling and control of vanadium redox flow battery for smoothing wind power fluctuation. IET Renewable Power Gener. 15(15), 3552–3563 (2021)
16. Trovò, A., Di Noto, V., Mengou, J.E., Gamabaro, C., Guarnieri, M.: Fast response of kW-class vanadium redox flow batteries. IEEE Trans. Sustainable Energy. 12(4), 2413–2422 (2021)
17. Paturet, M., Markovic, U., Delikaraoglou, S., Vrettos, E., Aristidou, P., Hug, G.: Stochastic unit commitment in low-inertia grids. IEEE Trans. Power Syst. 35(5), 3448–3458 (2020)
18. Zheng, Q.P., Wang, J., Liu, A.L.: Stochastic optimization for unit commitment—A review. IEEE Trans. Power Syst. 30(4), 1913–1924 (2014)
19. Mazidi, M., Monsef, H., Siano, P.: Design of a risk-averse decision making tool for smart distribution network operators under severe uncertainties: An IGDT-inspired augment ε-constraint based multi-objective approach. Energy. 116, 214–235 (2016)
20. Mohiti, M., Monsef, H., Anvari-Moghaddam, A., Lesani, H.: Two-stage robust optimization for resilient operation of microgrids considering hierarchical frequency control structure. IEEE Trans. Ind. Electron. 67(11), 9439–9449 (2019)
21. Doostizadeh, M., Aminifar, F., Ghasemi, H., Lesani, H.: Energy and reserve scheduling under wind power uncertainty: An adjustable interval approach. IEEE Trans. Smart Grid. 7(6), 2943–2952 (2016)
22. Nasr, M.-A., Nasr-Azadani, E., Nafisi, H., Hosseinian, S.H., Siano, P.: Assessing the effectiveness of weighted information gap decision theory integrated with energy management systems for isolated microgrids. IEEE Trans. Ind. Inf. 16(8), 5286–5299 (2019)
23. Soroudi, A., Rabiee, A., Keane, A.: Information gap decision theory approach to deal with wind power uncertainty in unit commitment. Electr. Power Syst. Res. 145, 137–148 (2017)
24. Ahmadi, A., Nezhad, A.E., Hredzak, B.: Security-constrained unit commitment in presence of lithium-ion battery storage units using information-gap decision theory. IEEE Trans. Ind. Inf. 15(1), 148–157 (2018)
25. Ahrabi, M., Abedi, M., Nafisi, H., Mirzaei, M.A., Mohammadi-Ivatloo, B., Marzband, M.: Evaluating the effect of electric vehicle parking lots in transmission-constrained AC unit commitment under a hybrid IGDT-stochastic approach. Int. J. Electr. Power Energy Syst. 125, 106546 (2020)
26. Kundur, P.: Power system stability. Power Syst. Stability Control 7–1 (2007)
27. Teng, F., Strbac, G.: Assessment of the role and value of frequency response support from wind plants. IEEE Trans. Sustainable Energy. 7(2), 586–595 (2016)

28. Nguyen, T.A., Qiu, X., Guggenberger, J.D. II, Crow, M.L., Elmore, A.C.: Performance characterization for photovoltaic-vanadium redox battery microgrid systems. IEEE Trans. Sustainable Energy. 5(4), 1379–1388 (2014)
29. Blanc, C., Rufer, A.: Multiphysics and energetic modeling of a vanadium redox flow battery. In: 2008 IEEE International Conference on Sustainable Energy Technologies, IEEE, pp. 696–701 (2008)
30. Gong, Q., Wang, Y., Fang, J., Qiao, H., Liu, D.: Optimal configuration of the energy storage system in ADN considering energy storage operation strategy and dynamic characteristic. IET Gener. Transm. Distrib. 14(6), 1005–1011 (2020)
31. Conejo, A.J., Castillo, E., Minguez, R., Garcia-Bertrand, R.: Decomposition Techniques in Mathematical Programming: Engineering and Science Applications. Springer Science & Business Media, New York (2006)
32. Trovò, A.: Battery management system for industrial-scale vanadium redox flow batteries: Features and operation. J. Power Sources. 465, 228229 (2020)
33. McDowall, J.: A guide to lithium-ion battery safety. Battcon. 1, 1–23 (2014)
34. Kermani, M., Adelmanesh, B., Shirdare, E., Sima, C.A., Carnì, D.L., Martirano, L.: Intelligent energy management based on SCADA system in a real Microgrid for smart building applications. Renewable Energy. 171, 1115–1127 (2021)
35. Thien, T., Axelsen, H., Merten, M., Axelsen, H., Zurmùhlen, S., Leuthold, M.: Planning of grid-scale battery energy storage systems: Lessons learned from a 5 MW hybrid battery storage project in germany. In: Proceedings of BATTCON International Battery Conference, pp. 18–1 (2015)
36. Hiskens, I.: IEEE PES task force on benchmark systems for stability controls. *Technical Report* (2013)
37. Ashouri-Zadeh, A., Toulabi, M., Dobakhshari, A.S., Ranjbar, A.M.: Frequency stability improvement in wind-thermal dominated power grids. IET Gener. Transm. Distrib. 14(4), 619–627 (2020)

How to cite this article: Mohiti, M., Mazidi, M., Kermani, M., Zarchi, D.A.:
Frequency-constrained energy and reserve scheduling in wind incorporated low-inertia power systems considering vanadium flow redox batteries. IET Gener. Transm. Distrib. 1–19 (2022).
https://doi.org/10.1049/gtd2.12592